The FEBS Journal

FEBS PRESS science publishing by scientists

Increased oxidative stress and CaMKII activity contribute to electro-mechanical defects in cardiomyocytes from a murine model of Huntington's disease

Julliane Vasconcelos Joviano-Santos[1], Artur Santos-Miranda[2], Ana Flávia Machado Botelho[3], Itamar Couto Guedes de Jesus[4], Jéssica Neves Andrade[1], Tatiane de Oliveira Barreto[2], Matheus Proença S. Magalhães-Gomes[1], Priscila Aparecida Costa Valadão[1], Jader dos Santos Cruz[2], Marília Martins Melo[3], Silvia Guatimosim[4] and Cristina Guatimosim[1]

1 Department of Morphology, Instituto de Ciências Biológicas, Universidade Federal de Minas Gerais, Belo Horizonte, Brazil
2 Department of Biochemistry and Immunology, Instituto de Ciências Biológicas, Universidade Federal de Minas Gerais, Belo Horizonte, Brazil
3 Department of Veterinary Clinic and Surgery, Escola de Veterinária, Universidade Federal de Minas Gerais, Belo Horizonte, Brazil
4 Department of Physiology, Instituto de Ciências Biológicas, Universidade Federal de Minas Gerais, Belo Horizonte, Brazil

Keywords
action potential; arrhythmia; CaMKII; Huntington's disease; oxidative damage

Correspondence
C. Guatimosim, Department of Morphology, Instituto de Ciências Biológicas, Universidade Federal de Minas Gerais, Av. Antônio Carlos, 6627 Belo Horizonte, MG, Brazil
Tel: +55 3134992824
E-mail: cguati@icb.ufmg.br

(Received 29 August 2018, revised 9 October 2018, accepted 15 November 2018)

doi:10.1111/febs.14706

Huntington's disease (HD) is a neurodegenerative genetic disorder. Although described as a brain pathology, there is evidence suggesting that defects in other systems can contribute to disease progression. In line with this, cardiovascular defects are a major cause of death in HD. To date, relatively little is known about the peripheral abnormalities associated with the disease. Here, we applied a range of assays to evaluate cardiac electro-mechanical properties *in vivo*, using a previously characterized mouse model of HD (BACHD), and *in vitro*, using cardiomyocytes isolated from the same mice. We observed conduction disturbances including QT interval prolongation in BACHD mice, indicative of cardiac dysfunction. Cardiomyocytes from these mice demonstrated cellular electro-mechanical abnormalities, including a prolonged action potential, arrhythmic contractions, and relaxation disturbances. Cellular arrhythmia was accompanied by an increase in calcium waves and increased Ca^{2+}/calmodulin-dependent protein kinase II activity, suggesting that disruption of calcium homeostasis plays a key part. We also described structural abnormalities in the mitochondria of BACHD-derived cardiomyocytes, indicative of oxidative stress. Consistent with this, imbalances in superoxide dismutase and glutathione peroxidase activities were detected. Our data provide an *in vivo* demonstration of cardiac abnormalities in HD together with new insights into the cellular mechanistic basis, providing a possible explanation for the higher cardiovascular risk in HD.

Abbreviations
AP, action potential; $APR_{90\%}$, 90% AP repolarization; CaMKII, Ca^{2+}/calmodulin-dependent protein kinase II; CAT, catalase; DCF, dichlorodihydrofluorescein diacetate; ECG, electrocardiography; F_0, baseline fluorescence; F, fluorescence; GAPDH, glyceraldehyde 3-phosphate dehydrogenase; GPx, glutathione peroxidase; HD, Huntington's disease; *Htt*, *huntingtin* gene; HTT, huntingtin; mHTT, mutant Huntingtin; PB, sodium phosphate buffer; PLN, phospholamban; polyQ, polyglutamine; ROS, reactive oxygen species; SERCA, sarco/endoplasmic reticulum Ca^{2+}-ATPase; SOD, superoxide dismutase; SR, sarcoplasmic reticulum.

Introduction

Huntington's disease (HD) is a neurodegenerative genetic disorder clinically characterized by progressive movement alterations, cognitive dysfunction, and psychiatric impairment [1,2]. The disease is an autosomal dominant condition caused by expansion of a CAG trinucleotide repeat sequence present in the *huntingtin* (*Htt*) gene, which results in an abnormally long polyglutamine (polyQ) tract in the N terminus of the huntingtin (HTT) protein [3]. A hallmark of HD is the clustering of mutant HTT (mHTT) as insoluble aggregates, which have been extensively associated with progressive neuronal death [4–6]. Moreover, the loss of normal function and/or the gain of toxicity of mHTT is also associated with the cellular dysfunction and degeneration observed in HD pathogenesis [7].

Cardiac dysfunction contributes to both mortality and morbidity of HD, with cardiovascular disease and heart failure being the second most common cause of death of the patients [8,9]. Studies performed in mice and *Drosophila* show that cardiomyocyte-specific expression of disease-causing HTT-polyQ [83 polyQ repeats (Q83) in mice and different polyQ repeat lengths (Q25, Q46, Q72, and Q103) in *Drosophila*] leads to severe heart failure. This suggests that the cardiovascular disturbances might be a consequence of direct cardiomyocyte abnormalities as well as improper autonomous nervous system input [10,11]. Moreover, it has been described that cardiac mHTT expression inhibited protein complexes such as mechanistic target of rapamycin complex 1 (mTORC1), limiting heart growth and reducing the heart's ability to compensate for chronic stress [12]. BACHD, a new mouse model of HD, showed functional differences between WT and BACHD hearts starting at 3 months of age, and the aged BACHD mice developed cardiac fibrosis and apoptosis [13]. It is important to highlight that these transgenic mice express the human gene of mHTT, and unlike other models, BACHD shows slower disease progression, and for this reason is a valuable and unique model to investigate the HD-like pathology in aged animals [14]. However, despite the clinical importance, the mechanisms involved in cardiac dysfunction in HD remain poorly understood. Indeed, previous studies [13] have not addressed the contribution of the electrical and mechanical function in the heart to the development of HD in 12-month-old animals.

In this work, we investigated electro-mechanical properties such as action potential (AP) and cardiac cell contractility to better understand the mechanisms underlying cardiac malfunction in the BACHD mouse model of HD. We also searched for ultrastructural changes in the cardiomyocytes of these animals. We found that the hearts from the BACHD mice exhibited marked electro-mechanical dysfunction associated with oxidative stress, which might be the trigger for severe arrhythmias. Moreover, we identified ultrastructural changes in the mitochondria and imbalance in the antioxidant system in the cardiomyocytes. Finally, we propose a pathway associated with Ca^{2+}/calmodulin-dependent protein kinase II (CaMKII) activity responsible for the electro-mechanical alterations observed in the BACHD cardiac cells.

Results

BACHD mice present significant changes in electrocardiography recordings

Considering that HD is a disorder of middle age and the main cause of death of the patients is related to cardiovascular defects [8,9], 12-month-old WT and BACHD mice were subjected to electrocardiography (ECG) to investigate the *in vivo* changes in the conduction of cardiac impulses. The spontaneous conduction disturbances seen in the BACHD mice included QT interval prolongation, ST-segment deviation, wandering pacemaker, and 'M'-shaped R wave (Fig. 1A). Additionally, the BACHD mice showed a significant prolongation of the QT interval (WT: 78.3 ± 2.9 ms; BACHD: 85.5 ± 1.9 ms; mean ± SEM) and ST-segment (WT: 0.08 ± 0.04 mV; BACHD: 0.26 ± 0.07 mV) (Fig. 1B,C). The analysis of the other electrocardiographic parameters revealed no significant difference between the two groups of mice (Table 1).

Ventricular myocytes from BACHD mice show electrical, mechanical, and calcium handling disturbances

In light of the *in vivo* changes in the electrocardiogram observed in the BACHD mice, we next investigated whether the ventricular myocytes from the BACHD mice presented electrical and mechanical abnormalities. To this end, we used three different but complementary approaches: the patch-clamp technique, analyses of cell contraction, and confocal microscopy.

The results obtained with the patch-clamp technique revealed that the BACHD ventricular cardiomyocytes have prolonged AP duration and alternans (Fig. 2A). Figure 2B,C shows that a statistical difference was found between the groups: 90% AP repolarization ($APR_{90\%}$) WT: 107.4 ± 21.9 ms (n = 22 cells); BACHD: 226.5 ± 33.2 ms (n = 27 cells); standard

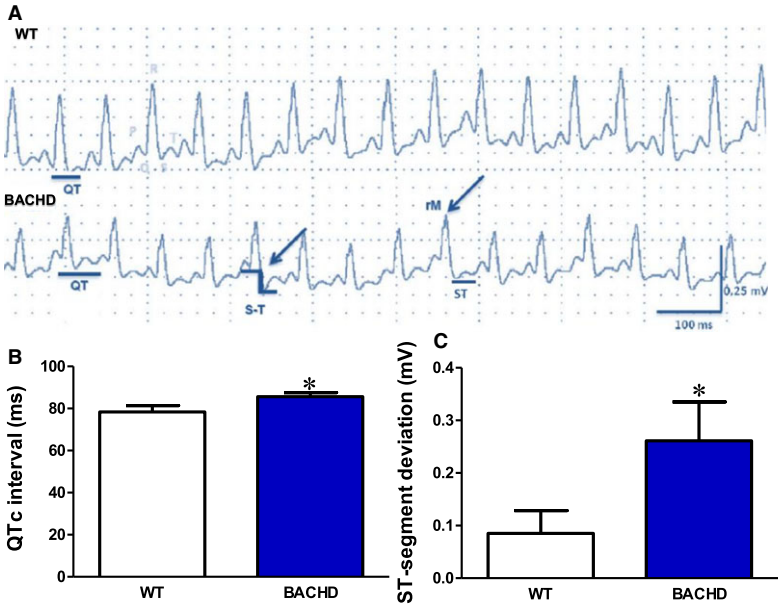

Fig. 1. Huntington's disease transgenic (BACHD) mice present electrocardiographic spontaneous electrical disturbances. (A) Electrocardiogram waveforms of WT (n = 10) and BACHD (n = 15) mice. BACHD mice presented QT interval prolongation, ST-segment elevation, and 'M'-shaped R wave (rM) (see arrows). (B) Bar graph showing a significant increase in QT interval in BACHD; QT interval was corrected by Van der Waters's formula (P = 0.04). (C) Bar graph showing a significant increase in the ST-segment elevation in BACHD compared with WT (P = 0.02). *P < 0.05, Student's t test. Data are expressed as mean ± SEM.

Table 1. Electrocardiography and cardiomyocyte AP parameters of WT and Huntington's disease transgenic (BACHD) mice. Data are expressed as mean ± SEM. No significant differences were observed between the groups (P > 0.05, Student's t test). bpm, beats per minute; HR, heart rate.

Parameter	WT	BACHD
ECG parameters		
P wave duration (ms)	31.9 ± 1.2	32.0 ± 1.2
P wave amplitude (mV)	0.03 ± 0.0	0.03 ± 0.0
PR interval (ms)	32.2 ± 0.9	33.3 ± 2.2
QRS duration (ms)	40.5 ± 0.9	42.5 ± 2.2
R wave amplitude (mV)	0.1 ± 0.01	0.1 ± 0.01
T wave amplitude (mV)	0.02 ± 0.0	0.02 ± 0.0
RR interval (ms)	0.1 ± 0.0	0.1 ± 0.0
HR (bpm)	499 ± 13	506 ± 9
AP parameters		
Maximum rise slope (dV/dt)	82.4 ± 11	81.8 ± 10
Resting membrane potential (mV)	−62.8 ± 0.6	−63.8 ± 0.6
AP amplitude (ms)	113.0 ± 2	110.9 ± 1

deviation of mean AP duration; mean σ for $APR_{90\%}$: WT: 9.1 ± 1.9 ms; BACHD: 64.9 ± 7.8 ms; mean ± SEM). Despite these changes, we did not find alterations in other AP parameters, i.e. maximum rise slope, resting membrane potential, and AP amplitude (Table 1).

Using the contraction assay, we noted that contraction in the WT cells was homogeneously synchronized with the electrical stimulus whereas the BACHD cardiomyocytes showed changes in the pattern of contraction (Fig. 3A). In fact, we observed a higher number of arrhythmic events (characterized by spontaneous contractions triggered without stimulation) in the BACHD cells. Figure 3B shows the number of arrhythmic events per 60 s in 50 WT cells and 53 BACHD cells (0.8 ± 0.4 and 4.8 ± 1.3, respectively, mean ± SEM). There was no alteration in the contractile parameters such as fractional shortening and maximum rate of contraction (Fig. 3C,D). However, we identified significant alterations in the relaxation parameters such as the maximum rate of relaxation, time to relaxation, and time to peak (Fig. 3E–G). Altogether, these data show the presence of arrhythmias at a cellular level and the preservation of contraction in spite of alterations in the relaxation parameters.

Next, we evaluated the Ca^{2+} dynamics in the BACHD ventricular cardiomyocytes. The cells were labeled with Fluo4 acetoxymethyl ester and imaged by confocal microscopy. We investigated the presence of calcium waves, the transient amplitude (F/F_0), and the rate of transient decay. As shown in Fig. 4A,B, BACHD cardiomyocytes presented an increased number of calcium waves when compared with WT. The calcium transient amplitude was maintained in the BACHD cardiomyocytes supporting the lack of alterations observed in the contraction (Fig. 4C). Finally, the decay constant was significantly decreased, corroborating the faster relaxation rate seen in the BACHD cells (Fig. 4D).

Molecular alterations in the ventricular myocardium of BACHD mice

To assess the molecular alterations of proteins involved in the excitation–contraction coupling, we performed

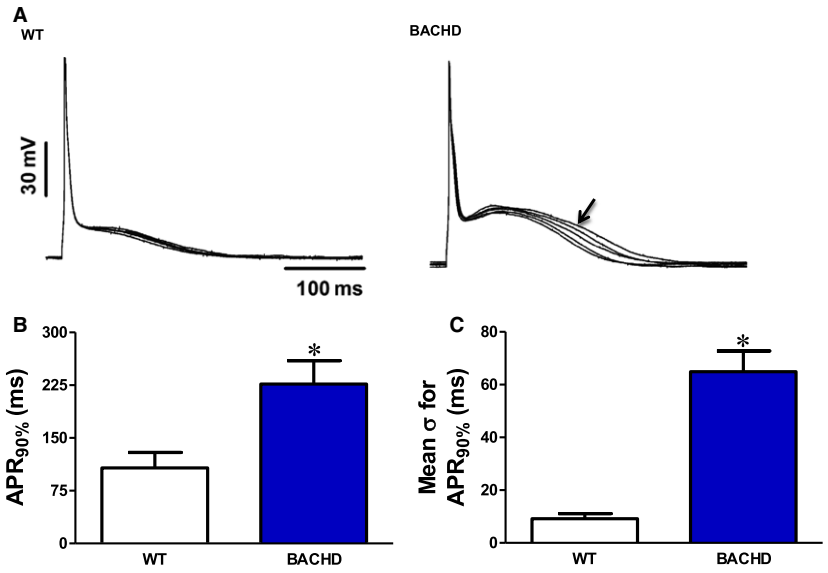

Fig. 2. Huntington's disease transgenic (BACHD) mice show alterations in AP in ventricular cardiomyocytes. (A) Representative AP traces obtained for WT and BACHD cardiomyocytes. In BACHD, the cardiomyocytes present a prolonged AP and AP duration alternans (arrow). (B) Bar graph showing significant increase in AP repolarization (APR) time in BACHD ($P = 0.009$). (C) Bar graph showing significant increase in AP duration alternans in BACHD ($P < 0.0001$). Sigma: Standard deviation of mean AP duration from 30 consecutive analyzed AP. Analyses involved $n = 22$ and $n = 27$ cells from four different WT and BACHD animals, respectively, in 10 consecutive beats. $^*P < 0.05$ compared with WT, Student's t test. Data are expressed as mean ± SEM.

western blotting of the ventricular myocardium samples (Fig. 5A). Figure 5B reveals that the expression of SERCA did not change between the groups (WT: 1.6 ± 0.2; BACHD: 1.7 ± 0.3; mean ± SEM). However, BACHD samples showed increased phosphorylation of phospholamban (PLN) at Thr17 (WT: 1.0 ± 0.04; BACHD: 1.6 ± 0.2; mean ± SEM) (Fig. 5C) and CaMKII at Thr^{286} (WT: 1.0 ± 0.1; BACHD: 2.2 ± 0.5; mean ± SEM) (Fig. 5D).

CaMKII is involved in the mechanical disturbances observed in cardiomyocytes from BACHD mice

Considering our data that showed increased CaMKII phosphorylation in the BACHD hearts and its role during the development of cardiac arrhythmias [15,16], we assessed CaMKII's contribution in the mechanical disturbances observed in the BACHD cardiomyocytes. We incubated the ventricular myocytes with the CaMKII inhibitor KN93 before the contractility assay. Although KN93 blocked cell arrhythmias (Fig. 6A), it did not affect cell fractional shortening and the maximum rate of contraction (Fig. 6B,C), in accordance with our previous results (described in Fig. 3). On the other hand, the maximum rate of relaxation, time to relaxation, and time to peak of BACHD cardiomyocytes were similar when compared with the WT KN93 group (Fig. 6D–F), indicating there was a reversal of the effects previously observed in these relaxation parameters (shown in Fig. 3). We did not observe such differences when using the inactive analog KN92.

BACHD mice present ultrastructural alterations in the ventricular myocardium associated with oxidative damage

Because CaMKII plays a key role in the development of arrhythmias in BACHD cells, we decided to investigate whether the BACHD cells presented any sign of oxidative damage since reactive oxygen species (ROS) can lead to CaMKII oxidation and consequently its activation. Therefore, we searched for evidence of oxidative stress in the ventricular myocardium using electron microscopy and found mitochondrial ultrastructural abnormalities. Accordingly, based on a qualitative analysis, the mitochondria of the ventricular myocardium were degraded and had absent cristae or were filled by granules (Fig. 7A–E). Although we also detected changes in the WT myocardium, these were less intense than the damage observed in the BACHD myocardium. Additionally, we observed the presence of lipofuscin granules in the cardiac tissue. Because the lipofuscin content may include aggregates of oxidized proteins [17] and, therefore, is indirect evidence of

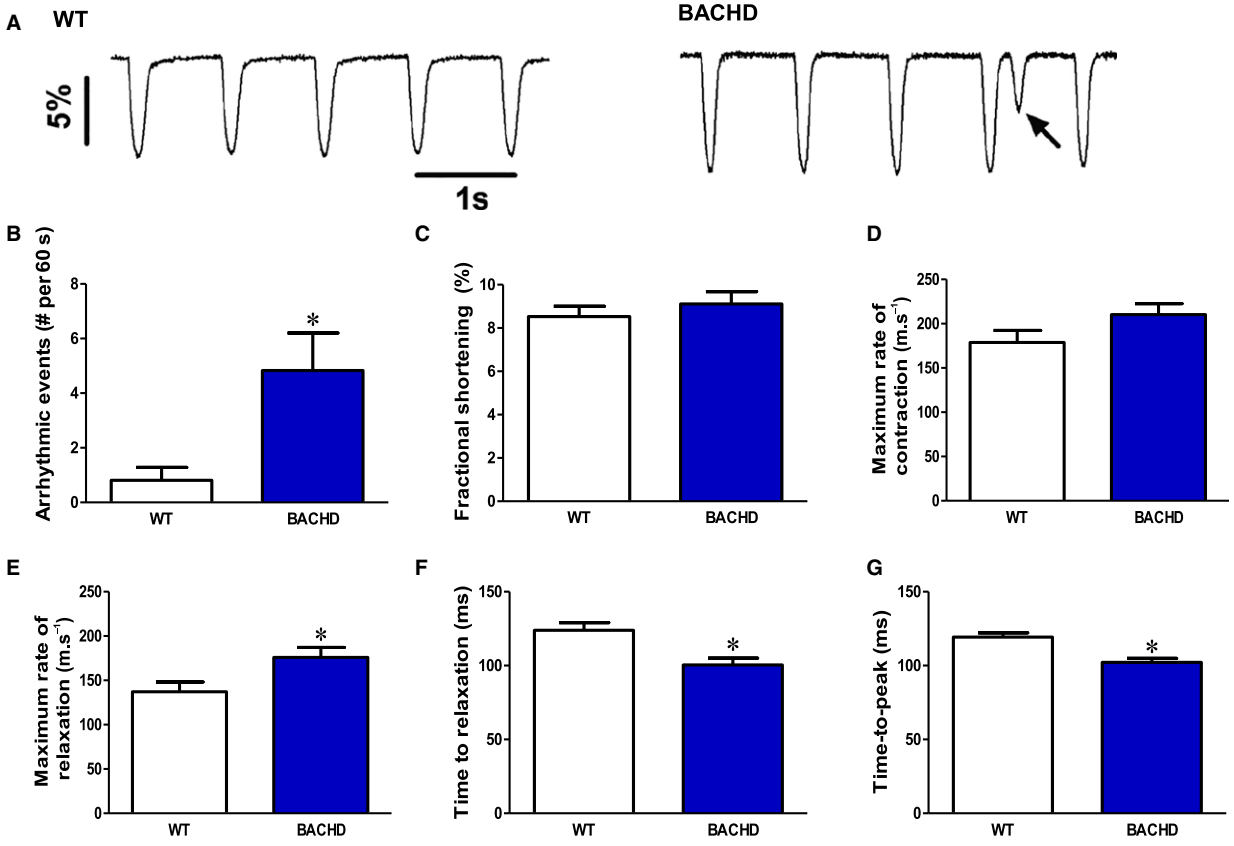

Fig. 3. Huntington's disease transgenic (BACHD) mice show mechanical changes in ventricular cardiomyocytes. (A) Representative contraction traces obtained from ventricular cardiomyocytes of WT and BACHD mice. The arrow shows arrhythmic events in BACHD cells. (B) Bar graph showing a significant increase in arrhythmic events in BACHD cells ($P = 0.004$). (C) Bar graph showing no alterations in fractional shortening ($P = 0.21$). (D) Bar graph showing no alterations in the maximum rate of contraction ($P = 0.37$). (E) Bar graph showing significant increase in the maximum rate of relaxation in BACHD cells ($P = 0.007$). (F) Bar graph showing a significant decrease in the time to relaxation in BACHD cells ($P = 0.0005$). (G) Bar graph showing significant decrease in the time-to-peak in BACHD cells ($P < 0.0001$). Analyses involved $n = 50$ and $n = 53$ cells from four different WT and BACHD animals, respectively. $^*P < 0.05$ compared with WT, Student's *t* test. Data are expressed as mean ± SEM.

oxidative stress, we quantified these granules and found that the BACHD myocardium presented a higher number of lipofuscin deposits than in the WT myocardium (Fig. 7F).

The analyses of the cardiac antioxidant system revealed an increase in the superoxide dismutase (SOD; Fig. 8A) and glutathione peroxidase (GPx; Fig. 8C) activities and no alteration in the catalase (CAT) activity (Fig. 8B), supporting the hypothesis that oxidative damage is likely to underlie the alterations observed in the BACHD myocardium. And finally, with two different probes we observed a significant increase in the fluorescence of BACHD cells, suggesting oxidative stress [dichlorodihydrofluorescein diacetate (DCF) in Fig. 8D: WT: 13.9 ± 1.0 A.U.; BACHD: 65.3 ± 4.5 A.U.; MitoSOX in Fig. 8E: WT: 21.3 ± 0.9 A.U.; BACHD: 26.3 ± 1.2 A.U.; mean ± SEM].

Discussion

We investigated the electrical function of middle-aged BACHD mouse hearts as well as excitability, contractility, and Ca^{2+} handling aspects of the freshly isolated ventricular cardiomyocytes from these mice. In this study, we revealed that the mouse model of HD presents electrocardiographic abnormalities (e.g. QT interval prolongation and ST-segment elevation). These ECG parameters are indicative of a delay in ventricular repolarization and ventricular overload that may be caused by hypoxia, myocardial infarction, or oxidative stress [18]. Our results are in accordance with the study of Schroeder *et al.* [13], which showed ST-segment range and elevation in BACHD mice, despite the fact that they used a different background (C57BL6/J). Importantly, many drugs prescribed to

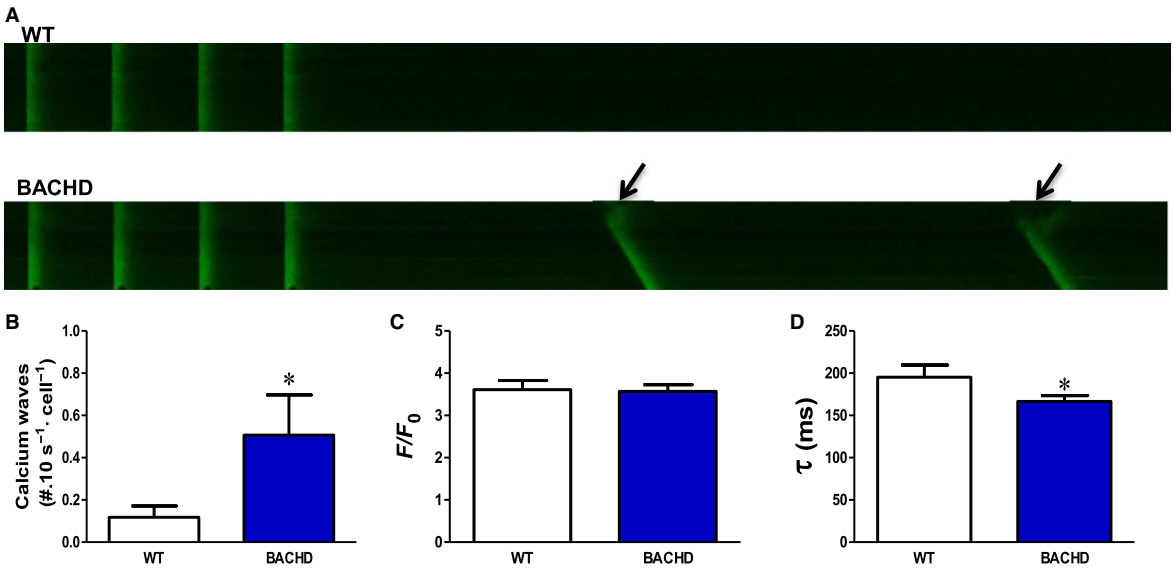

Fig. 4. Huntington's disease transgenic (BACHD) mice showed alterations in the intracellular calcium handling of ventricular cardiomyocytes. (A) Representative images of calcium transients from WT and BACHD mice observed by confocal microscopy. Calcium waves in BACHD cells are indicated by the arrows. (B) Bar graph showing a significant increase in the number of calcium waves in BACHD cells ($P = 0.004$). (C) Bar graph showing no alterations in calcium transient amplitude (F, fluorescence; F_0, basal fluorescence) ($P = 0.31$). (D) Bar graph showing a significant decrease in the decay rate in BACHD cells ($P = 0.01$). Analyses involved $n = 50$ and $n = 69$ cells from four different WT and BACHD animals, respectively. *$P < 0.05$ compared with WT, Student's t test. Data are expressed as mean ± SEM.

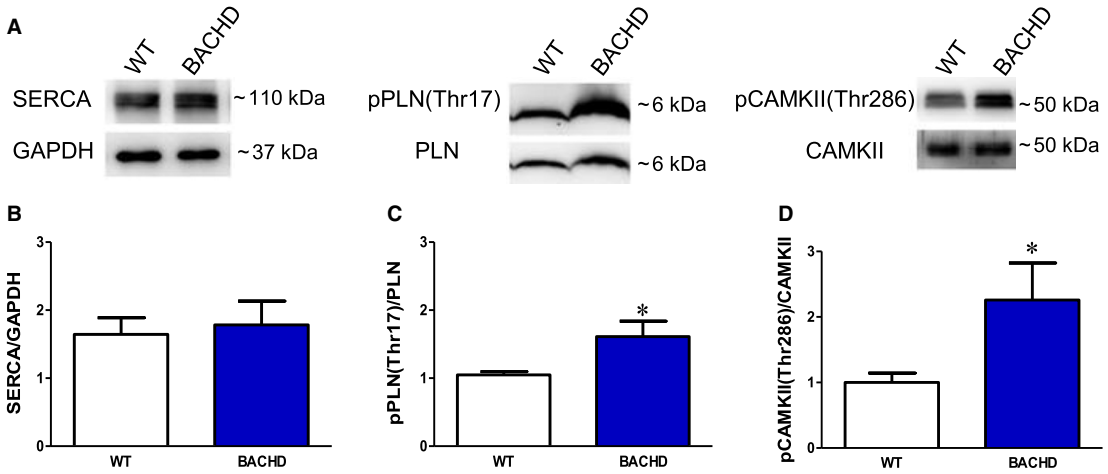

Fig. 5. Huntington's disease transgenic (BACHD) mice showed alterations in key proteins involved in excitation–contraction coupling in ventricular myocardium. (A) Representative western blotting of SERCA, pPLNThr17/PLN, and pCaMKIIThr286/CaMKII immunodetection of ventricular myocardium samples obtained from WT and BACHD mice. (B) Bar graph showing no alterations in SERCA expression ($P = 0.30$). (C) Bar graph showing a significant increase in the expression of pPLNThr17/PLN in BACHD ventricular myocardium ($P = 0.04$). (D) Bar graph showing a significant increase in the expression of pCaMKIIThr286/CaMKII expression in BACHD hearts ($P = 0.03$). The analyses involved eight animals per group. *$P < 0.05$ compared with WT, Student's t test. Data are expressed as mean ± SEM.

HD patients to treat some symptoms, but not to modify the disease progression (e.g. thioridazine or haloperidol for psychosis), have a well-recognized potential to induce QT prolongation as a side effect [19]. Delayed ventricular repolarization is associated with the development of severe arrhythmias [20], prominently ventricular tachycardia such as torsades de pointes. The association of these drugs with prolonged QT interval might increase the patient's risk of developing severe electrical disturbances and/or sudden

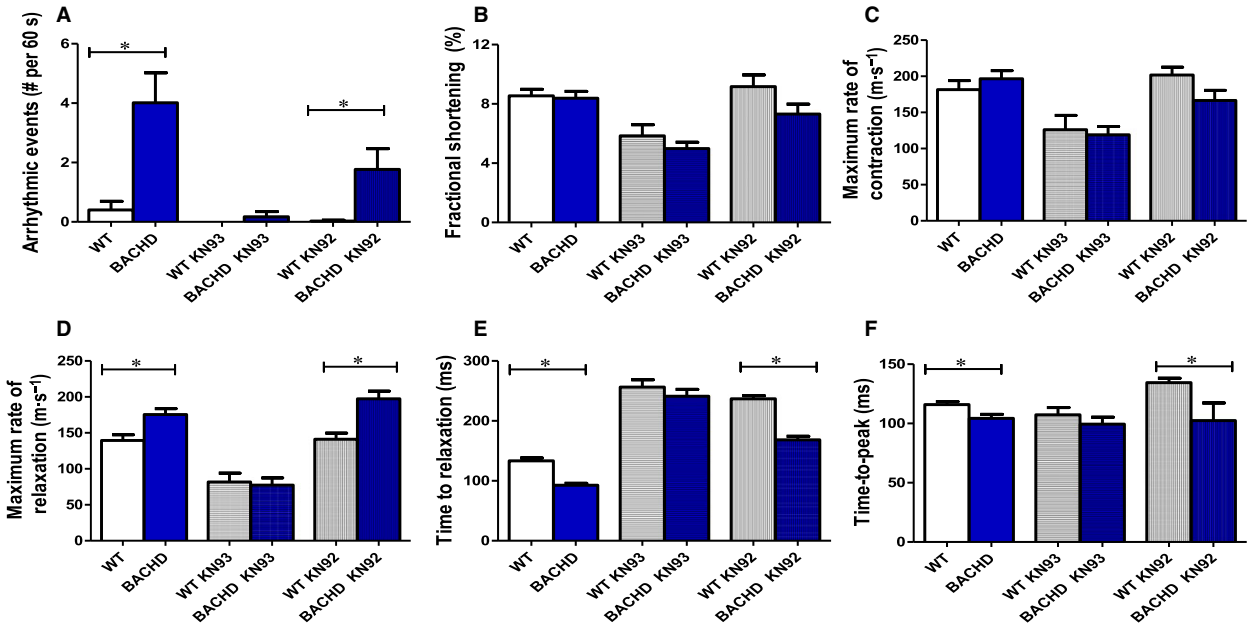

Fig. 6. Mechanical changes in the cardiomyocytes of Huntington's disease transgenic (BACHD) mice are mediated by CaMKII activity. (A) Bar graph showing inhibition of arrhythmic events after incubation of BACHD mouse cardiomyocytes with KN93. (B) Bar graph showing no alterations in fractional shortening after incubation of cardiomyocytes with KN93. (C) Bar graph showing no alterations in the maximum rate of contraction after incubation of cardiomyocytes with KN93. (D) Bar graph showing an increased relaxation in BACHD mouse cardiomyocytes that were not treated with KN93 and the absence of alterations in the cardiomyocytes treated with KN93 in comparison with the respective WT controls. (E,F) Bar graphs showing decreased time to relaxation (E) and time-to-peak (F) in BACHD mouse cardiomyocytes that were not treated with KN93, and the absence of alterations in BACHD mouse cardiomyocytes treated with KN93 in comparison with the respective WT controls. KN92 is an inactive analog and it was used to control for off-target effects of KN93. The same differences between WT and BACHD were also observed when comparing WT KN92 and BACHD KN92 groups. $*P < 0.05$ BACHD, BACHD KN93 and BACHD KN92 groups compared with the respective WT controls. Analyses involved WT $n = 57$, BACHD $n = 70$, WT KN93 $n = 38$, BACHD KN93 $n = 46$, WT KN92 $n = 34$ and BACHD KN92 $n = 30$, cells from four different WT and BACHD animals. One-way ANOVA followed by Newman–Keuls test. Data are expressed as mean ± SEM.

cardiac death. Interestingly, apart from the above observations, we did not detect abnormalities in the conduction of atrial cardiac impulses and ventricular depolarization.

Following the *in vivo* ECG observations, we evaluated the excitation–contraction properties of the ventricular cardiomyocytes. The AP repolarization phase of the BACHD cardiomyocytes was delayed, in accordance with the observed prolonged QT interval. Furthermore, BACHD cardiomyocytes showed AP duration alternans, which is a risk factor for the development of different types of arrhythmic events [21,22] that can lead to several ventricular arrhythmias and atrial fibrillation [23]. It is possible that the prolongation of AP favors re-entry phenomena that allow repetitively excitable circuits [23]. It is important to highlight that triggered arrhythmias and re-entrant mechanisms likely co-exist, especially in structurally diseased heart tissue. We suggest that, in BACHD cardiomyocytes, prolonged AP together with the increased AP duration alternans provides a favorable substrate for severe arrhythmias, which in turn might contribute to an impaired heart function and finally heart failure [22], known to occur in HD patients [8].

The increase in AP duration alternans led us to investigate the intracellular calcium dynamics because calcium affects the maintenance of excitability and contraction in cardiomyocytes [22]. The BACHD cells presented a higher number of Ca^{2+} waves than those of WT mice, suggesting an increased leak of calcium from ryanodine receptors. Increase in the calcium leak promotes the calcium-dependent depolarization of cardiomyocyte membranes through Na^{+}/Ca^{2+} exchanger activity, a process that may account for the prolonged AP and could also determine the appearance of the early depolarization events [24,25] corroborating the increased arrhythmia discussed above. Indeed, increased arrhythmic contractions that appear independent of triggered stimulation were detected by the edge detection assay tracking cell contraction, further strengthening this idea.

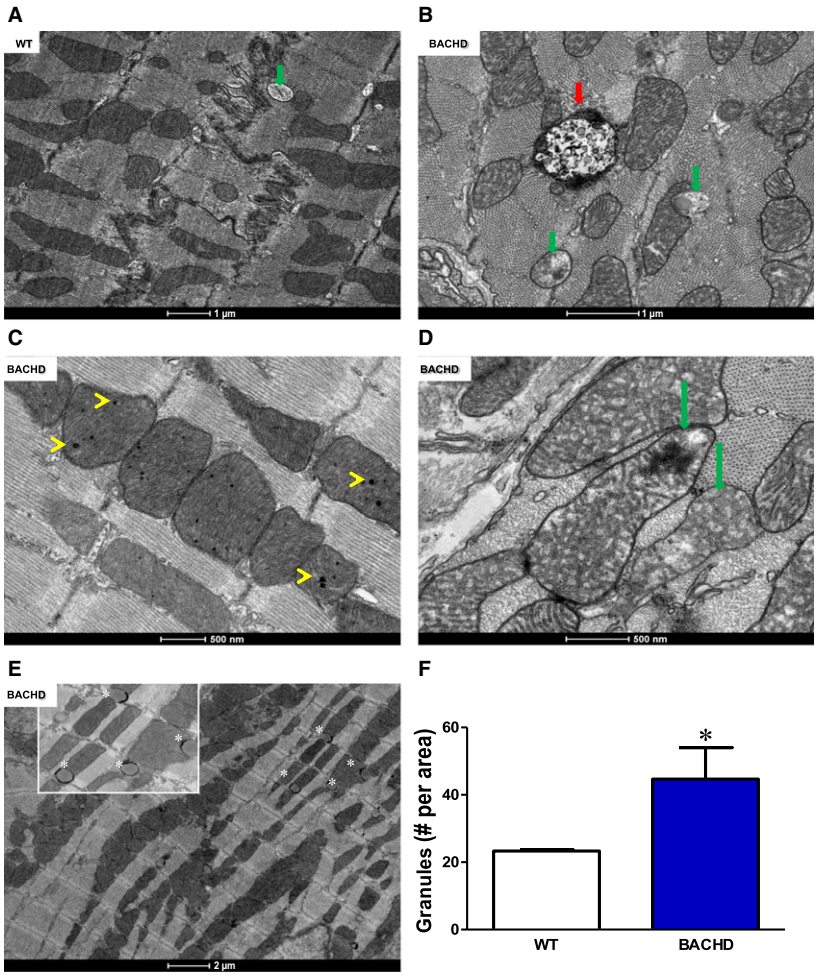

Fig. 7. Ventricular myocardium of Huntington's disease transgenic (BACHD) mice show pronounced mitochondrial ultrastructural abnormalities. (A) Representative electron micrograph of ventricular myocardium of WT mice. (B–E) Representative electron micrographs of ventricular myocardium of BACHD mice revealing ultrastructural abnormalities: severe mitochondrial damage presented by altered or absent cristae (green arrows); presence of lipofuscin granules (red arrows); intramitochondrial granules (yellow arrowheads) and lipid bodies (white asterisks and shown in inset). (F) Bar graph showing a significant increase in number of lipofuscin granules in the ventricular myocardium of BACHD mice ($P = 0.03$). Thirty images obtained from three animals per group were analyzed. *$P < 0.05$ compared with WT, Student's *t* test. Data are expressed as mean ± SEM.

Despite the strong evidence of increased calcium leak from RyRs, the calcium transient amplitude remained unaltered in accordance with the unchanged cellular fractional shortening. At first glance, such a finding may appear controversial since a reduction in calcium, in response to the increase in calcium leak, impairs the balance between calcium influx and uptake from the sarcoplasmic reticulum (SR) [20,26]. However, we also observed a decrease in the calcium transient decay rate and an increase in the relaxation speed, suggesting a rise of SERCA activity [27] that could compensate for the proposed increase in the calcium leak. Corroborating this assumption, we found a significant increase in PLN^{Thr17} phosphorylation. It is known that phosphorylation of PLN by protein kinase A and/or CaMKII (in addition to other kinases) progressively removes its ability to inhibit SERCA activity [27]. This finding may determine an increase in SERCA activity, increasing transport of Ca^{2+} to the SR interior, which may reflect an increase in the relaxation rate and calcium reuptake by the SR. In agreement with the aforementioned data, we also observed a rise in the levels of CaMKII protein, determining the increased phosphorylation at the Thr^{17} site of PLN.

CaMKII is a calcium and calmodulin-regulated enzyme and multifunctional serine/threonine protein kinase with widespread expression in the muscle, nervous and immune tissues [27,28]. However, post-

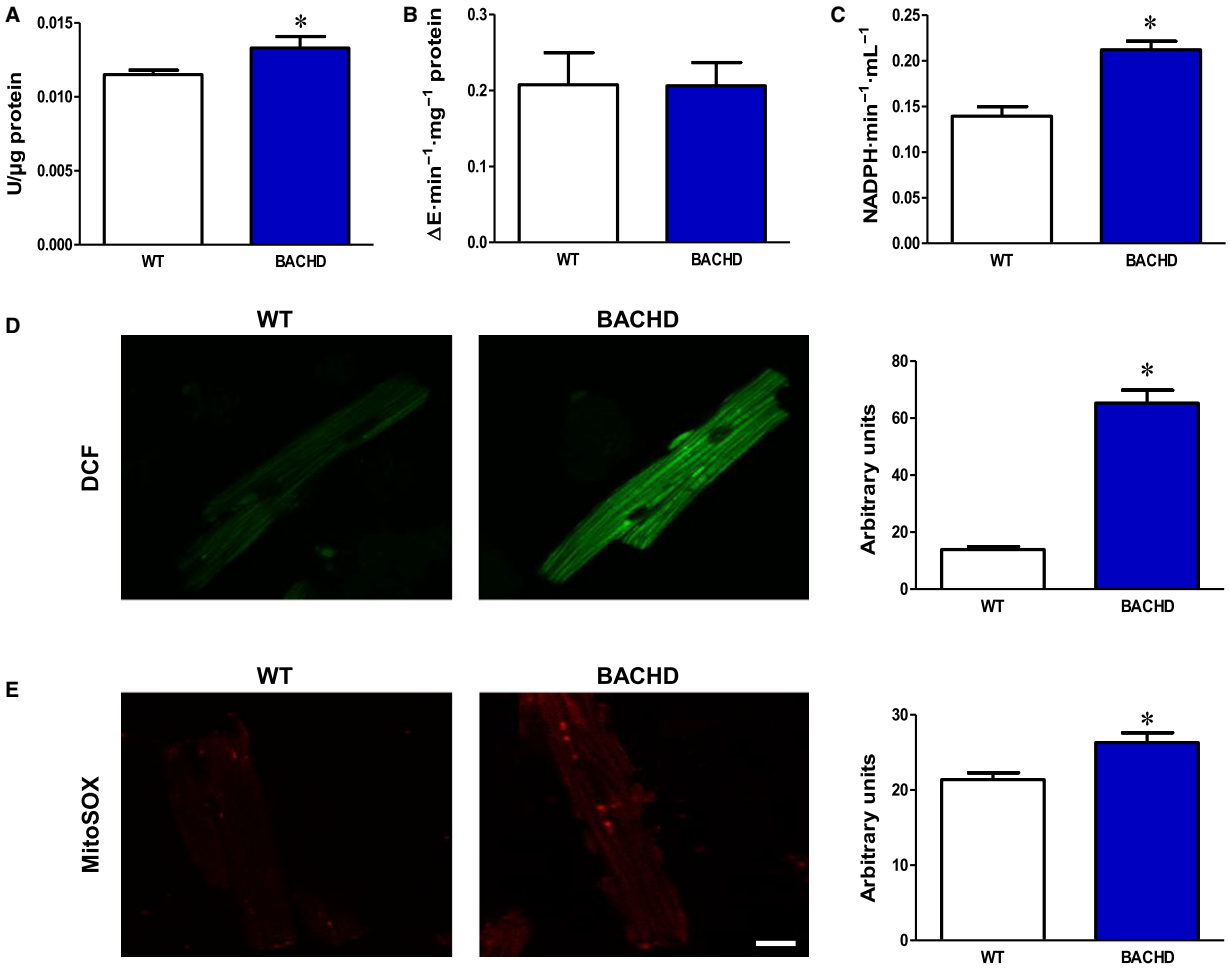

Fig. 8. Ventricular myocardium of Huntington's disease transgenic (BACHD) mice shows changes in antioxidant systems and oxidative stress. (A) Bar graph showing significant increase in SOD activity in BACHD myocardium ($P = 0.01$). (B) Bar graph showing no alterations in CAT activity in both groups ($P = 0.50$). (C) Bar graph showing significant increase in GPx activity in BACHD mouse myocardium ($P = 0.001$). The analyses involved 10 animals per group. (D) Representative cardiomyocytes from WT and BACHD mice, and bar graph showing an increase in DCF labelling ($P < 0.0001$). (E) Representative cardiomyocytes from WT and BACHD mice, and bar graph showing an increase in MitoSOX labelling ($P = 0.001$). DCF, $n = 106$ and $n = 120$ cells, and MitoSOX, $n = 101$ and $n = 103$ cells from three WT animals and three BACHD animals, respectively. Scale bar: 25 µm. *$P < 0.05$ compared with WT, Student's t test. Data are expressed as mean ± SEM.

translational modifications can convert CaMKII to a calcium and calmodulin-independent enzyme involved in some cardiovascular disease, including during arrhythmogenic episodes [27]. CaMKII can be super-activated under pathological conditions including acidosis, ischemia, and oxidative stress [28,29]. Moreover, this enzyme mediates arrhythmias in chronic diseases such as during heart failure and in genetic syndromes such as long-QT syndrome [29]. To confirm the involvement of CaMKII in the deleterious effects observed in the function of the BACHD cardiomyocytes, we incubated these cells with KN93, a direct inhibitor of CaMKII [30]. Strikingly, KN93 abolished arrhythmic contractions and restored the rate of relaxation, time to relaxation, and time to peak to the levels observed in WT KN93-treated cells. It is noteworthy that KN93 promoted a slight reduction in the cell fractional shortening in the cardiomyocytes of WT and BACHD mice, indicating that CaMKII is an important modulator of cellular electro-mechanical properties, in accordance with previous findings [28,29]. We also used the inactive analog KN92 to control for off-target effects of KN93. The same differences between WT and BACHD were also observed when comparing WT KN92 and BACHD KN92 groups, corroborating the KN93 action. As suggested by Mustroph *et al.* [29], strategies aiming to alter CaMKII expression and/or activity could be a new

approach to prevent arrhythmias as well as systolic and diastolic ventricular dysfunctions.

Under oxidative conditions, high ROS can enhance the CaMKII activity by direct or indirect pathways [28]. We investigated the oxidative damage status (associated with ROS) of BACHD myocardium. Based on a qualitative analysis of mitochondria in the ventricular myocardium, mitochondria were degraded in the BACHD group. It is well known that mitochondrial changes and lipofuscin accumulation are important features of aging in non-mitotic cells [31,32], such as neurons and cardiomyocytes. Terman *et al.* [32] showed a positive correlation between the intracellular lipofuscin content and both mitochondrial damage and production of ROS. Thus, considering that mitochondria are significant sources of ROS production and that enhanced lipofuscinogenesis is strongly related to oxidative enzymatic activity, we investigated how some key components of the cellular antioxidant system were operating in HD.

The differences in the oxidative status of the cardiac cells were examined by evaluating the antioxidant defense system through SOD, CAT, and GPx activities. Normally, SOD activity is the first line of defense against the superoxide anion $O_2^{\cdot-}$ leading to the release of H_2O_2 and O_2. Another component responsible for decreasing the H_2O_2 production as well as for reducing the oxidized proteins is CAT. The increase in SOD and GPx activities, in association with the ultrastructural changes seen in the mitochondria, strongly indicates that oxidative disturbances are taking place in the cardiac tissue of the BACHD mice. In fact, oxidative stress in nervous tissue has a critical role in the pathogenesis of HD [8,33,34]. Importantly, using a direct assessment, we confirmed the oxidative stress in HD cardiomyocytes.

In conclusion, in this study, we demonstrated that elderly BACHD mice present abnormalities in cardiac repolarization as observed in the ECG profile, which translate into a prolonged duration of AP with enhanced AP duration alternans in isolated ventricular myocytes. The isolated cardiomyocytes further exhibit arrhythmic contraction and relaxation disturbances that are in accordance with the calcium handling imbalances, such as the increase in the number of calcium waves and Ca^{2+} reuptake, associated with SERCA activity and modulated by phosphorylated PLN. These effects can be explained by the heightened CaMKII expression and stimulation, as a consequence of oxidative stress, evidence that is supported by mitochondrial ultrastructural disorganization associated with the increase in the cellular antioxidant axis function and with the direct analyses of general oxidative stress and mitochondrial superoxide anion production indicators.

Although HD is a neurodegenerative condition, patients die primarily due to pulmonary complications followed by impairment of cardiovascular function [9]. Therefore, research into HD-associated cardiac dysfunctions and the mechanisms associated with them are relevant to a better understanding of HD pathophysiology. Most studies on HD have focused on the changes incurred in the nervous system. HD has a known genetic cause, a mutation in the *Htt* gene, and the BACHD mouse is an excellent model for neurodegenerative research. The findings presented herein may also be important to researchers interested in the cardiac aspects of others neurodegenerative disorders.

Materials and methods

Animals

FVB/NJ (WT) and FVB/N-Tg (HTT*97Q)IXwy/J (BACHD) transgenic mice were purchased from The Jackson Laboratory (Bar Harbor, ME, USA) and used to establish a new colony. For this study, we used 12-month-old wild-type (WT) and BACHD mice, when the HD-related phenotypes were shown to be more developed [14]. The animals were housed in a room with controlled humidity, temperature (23 ± 2 °C), and a 12-h light–dark cycle with free access to food and water. The experimental procedures were approved by the animal welfare committee of the Universidade Federal de Minas Gerais (CEUA-UFMG 25/2015).

In vivo procedures

The *in vivo* heart electrical impulse conduction was analyzed by ECG. A six-channel non-invasive electrocardiograph (ECG-PC version 2.07; TEB, São Paulo, Brazil) was used. WT ($n = 10$) and BACHD ($n = 15$) animals were anesthetized with 1.5–2.0% isoflurane inhalation (VetCase, Brasmed, Brazil) and recordings made at 50 mm·s^{-1} and 2 N. Data analysis of heart rate, segments, and intervals was conducted in lead II (DII).

Isolated ventricular cardiomyocytes

For *in vitro* analyses, ventricular cardiomyocytes from the mice ($n = 4$ mice per group) were isolated as previously described [35]. The animals were euthanized after heparinization (heparin 50 U, i.p.). Then, the heart was quickly dissected out and cannulated in a home-made constant-pressure Langendorff system through the aortic trunk. CIB nurturing solution (in mM: 30 NaCl; 5.4 KCl; 0.5 $MgCl_2$; 0.33 NaH_2PO_4; 25 HEPES; and 22 glucose) was perfused through the coronary system followed by the perfusion of an enzyme mix added to CIB in an increasing calcium concentration gradient. Then, freshly isolated cells were centrifuged, and

the resulting pellet was re-suspended in Tyrode's solution (in mM: 140 NaCl; 5.4 KCl; 0.5 $MgCl_2$; 0.33 NaH_2PO_4; 1.8 $CaCl_2$; 5 glucose; and 11 HEPES). The isolated ventricular cardiomyocytes were used for electrophysiology, cell contraction assay, and confocal microscopy.

Electrophysiology

Electrophysiological recordings of the cardiomyocyte AP were obtained using an EPC9.2 patch-clamp amplifier (HEKA, Harvard Bioscience, Inc., Holliston, MA, USA) in whole-cell current-clamp mode. The APs of 22 WT and 27 BACHD cardiomyocytes were recorded. After establishing this configuration, the cells were maintained at rest for 3 min for the pipette solution to equilibrate with the intracellular environment. Glass pipettes with tip resistances varying between 1 and 2 MΩ were used. The APs in the isolated ventricular cells were measured by applying a 1000 pA pulse lasting 2–4 ms with 1 Hz frequency.

Cell contractility assay

For the analyses of the cellular arrhythmias and contraction, the ventricular cardiomyocytes obtained from the WT ($n = 50$) and BACHD ($n = 53$) mice were placed on a coverslip coupled to a chamber containing a pair of parallel electrodes and stimulated electrically using 60 V biphasic pulses at 1 Hz for 4 ms [36]. Throughout these experiments, the cells were kept in Tyrode's solution at room temperature (25–30 °C). The cells were monitored through an MCS100 CCD camera (IonOptix, Milton, MA, USA), and the acquired images were used to measure cell shortening (contractility index) in response to the electrical stimulus using an edge detector video system. The images were obtained using an acquisition frequency of 240 Hz. Cell shortening was calculated based on the output obtained from the edge detection converter system IonWizard A/D. In some experiments (in another group of animals), we pretreated the cells with KN93 or KN92 (10 $\mu mol \cdot L^{-1}$; Sigma-Aldrich, St Louis, MO, USA) for 20 min without light.

Confocal microscopy

The alterations in the calcium handling were investigated by confocal microscopy using a Zeiss confocal microscope LSM 510 system (Zeiss, Jena, Germany). For these experiments, the cells were labeled with 5 μM Fluo4-AM for 30 min at 25 °C under gentle agitation. The labeled cells were excited with 60 V biphasic pulses at 1 Hz frequency for 4 ms. The scan line (set at 512 pixels) was positioned along the longitudinal axis to avoid nuclear regions. The spatial resolution ranged from 0.1 to 0.3 $\mu m \cdot pixel^{-1}$, and the temporal resolution used was 1.92 ms per line. The changes in fluorescence (F) were normalized with the baseline fluorescence (F_0). The data were recorded and analyzed using the software IMAGE-J (NIH, National Institutes of Health, Bethesda, MD, USA). Ca^{2+} transient amplitudes were taken as the mean between three transient recordings after a train of 10 pulses intended to load the SR. The calcium waves were analyzed by counting the number of waves during the 10 s after the acquisition of calcium transients, maintaining the cell at rest [36].

Western blot analyses

We used western blotting to analyze the protein expression. To this end, the left ventricles from the WT and BACHD mice ($n = 8$ animals per group) were homogenized in ice-cold lysis buffer (in mM: 100 NaCl, 50 Trizma base, 5 Na_2-EDTA, 50 $Na_4P_2O_7.10\ H_2O$; and 1 $MgCl_2$; pH 8.0) containing 0.3% Triton X-100, 1% NP-40, 0.5% sodium deoxycholate, and enriched with a cocktail of protease and phosphatase inhibitors. Next, 40–60 μg of protein was separated by SDS/PAGE followed by electronic transfer onto a PVDF membrane (Millipore, Darmstadt, Germany). The membranes were incubated with the following primary antibodies: anti-sarco/endoplasmic reticulum Ca^{2+}-ATPase (SERCA) (1 : 2500; Santa Cruz Biotechnology, Dallas, TX, USA), anti-PLN (Abcam, Cambridge, UK, 1 : 1500), anti-p-phospholamban-Thr^{17} (1 : 2500; Santa Cruz Biotechnology), anti-CaMKII (1 : 500; Santa Cruz Biotechnology), anti-pCaMKII Thr^{286} (1 : 500; Santa Cruz Biotechnology) and anti-glyceraldehyde 3-phosphate dehydrogenase (GAPDH) (1 : 3000; Santa Cruz Biotechnology). The immunodetection was carried out using enhanced chemiluminescence (GE Healthcare, Chicago, IL, USA) followed by densitometric analyzes with the software IMAGEQUANTTL (GE Healthcare). The protein levels were expressed as a ratio of the optical densities. GAPDH was used as a control for any variations in the protein loading.

Transmission electron microscopy

For qualitative ultrastructural analyses, the mice were anesthetized and transcardially perfused with sodium phosphate buffer (PB) and Karnovsky fixative solution. Next, the hearts from three animals from the WT and BACHD groups were removed, and the left ventricles were separated. The samples were washed with cacodylate buffer (0.1 M), post-fixed in reduced osmium (1% osmium tetroxide containing 1.6% potassium ferrocyanide), contrasted *en bloc* with uranyl acetate (2% uranyl acetate in deionized water), dehydrated through an ascending series of ethanol solutions, and embedded in EPON. Serial ultrathin sections were collected on 200- or 300-mesh copper grids and contrasted with lead citrate. The sections were viewed with a Tecnai-G2-Spirit FEI/Quanta electron microscope (120 kV; Philips, FEI Company, Hillsboro, OR, USA) maintained at the Microscopy Center – UFMG.

Antioxidant enzyme assays

For the antioxidant enzyme assays, the left ventricle samples obtained from the WT and BACHD mice (n = 10 animals per group) were weighed and homogenized (Euro Turrax T20b; IKA LABORTECHNIK, Wilmington, NC, USA) on ice in 0.2 g·mL^{-1} of PB at pH 7.2. The homogenates were centrifuged for 15 min at 10 000 ***g***, and the supernatant was used to quantify the SOD and CAT activities. The left ventricle samples were homogenized in ice-cold Tris/HCl buffer (50 mM, pH 7.5, containing 5 mM EDTA) and centrifuged at 4 °C (10 000 ***g***) for 20 min to measure the GPx activity. The protein concentration was determined using bovine serum albumin as the standard. Then, the following procedures were performed.

Superoxide dismutase activity

Superoxide dismutase activity was determined by measuring the inhibition of pyrogallol autoxidation, where 1 U = 50% pyrogallol inhibition autoxidation [37]. To this end, after the homogenization, the supernatant was collected and combined with PB containing 1.25 mM MTT and 100 mM pyrogallol at pH 7.2. After 5 min of incubation, the reaction was quenched by the addition of DMSO, and the reading was carried out at 570 nm.

Catalase activity

Catalase activity was determined by the decomposition of H_2O_2 following absorbance at 240 nm and expressed as millimoles of H_2O_2 decomposed per minute per milligram of protein ($\Delta E \cdot min^{-1} \cdot mg^{-1}$ protein). To this end, 0.05 mL homogenate supernatant was added to 50 mM PB (2 mL, pH 7.0, 25 °C). The reaction was started by adding H_2O_2 (6 mM) and allowed to proceed for 1 min at room temperature.

Glutathione peroxidase activity

The supernatant (4 μL) was added to 0.2 mL of PB (100 mM, pH7.5), with 2 mM reduced glutathione, 0.1 U·mL^{-1} glutathione reductase, 0.12 mM NADPH, 2 mM H_2O_2, and 1 mM sodium azide. The GPx activity was measured at 340 nm and expressed in nmol NADPH·min^{-1}·mL^{-1}.

Assessment of oxidative stress

For a direct assessment of oxidative stress in cardiac myocytes, confocal imaging was performed using a Zeiss LSM 880 at Center for Acquisition and Image Processing (CAPI, Federal University of Minas Gerais, Brazil). Freshly isolated cardiomyocytes were loaded with (a) DCF, a general oxidative stress indicator (2 μM, incubated for 20 min at room temperature), and (b) MitoSOX, an indicator of mitochondrial superoxide anion production (5 μM, incubated 150 ***g*** for 30 s) and bathed in Tyrode solution. The optical slice was set to 2 μm in all recorded images. Fluorescence was quantified on digitized pictures as the average of pixels of single focused cells (DCF, n = 106 and n = 120 cells, and MitoSOX, n = 101 and n = 103 cells from three WT and three BACHD animals, respectively). Fluorescence measurements are presented as the subtraction between cell fluorescence, excluding nuclei, and background fluorescence.

Statistical analysis

Data are expressed as mean ± standard error of mean (SEM). After the normality tests, the data were analyzed using Student's t test for comparing two groups and one-way ANOVA followed by the Newman–Keuls test for comparing more than two groups. All analyses were performed using PRISM 6 (GraphPad Software, La Jolla, CA, USA). The significance level was set to 5% ($P < 0.05$).

Acknowledgements

The authors would like to acknowledge the Center of Acquisition and Processing of Images (CAPI) – ICB – Universidade Federal de Minas Gerais and Microscopy Center at Universidade Federal de Minas Gerais for providing the equipment and technical support for experiments involving microscopy. This work was supported by grants from FAPEMIG (no. 00271-13 and no. -00801-16), CNPq (no. 467220/2014-0 and no. 475735/2013-7) and CAPES. CG and SG are Bolsista de Produtividade em Pesquisa (CNPq).

Conflict of interest

All authors declare no conflict of interest.

Author contributions

JVJ-S, AS-M, AFMB, ICGJ, JNA, TOB, MPSM-G, and PACV participated in acquisition, analysis, or interpretation of data for the work; and wrote the paper. JSC, MMM, SG, and CG participated in conception or design of the work; and drafting the work or revising it critically for important intellectual content.

References

1 Xuereb JH, MacMillan JC, Snell R, Davies P & Harper PS (1996) Neuropathological diagnosis and CAG repeat expansion in Huntington's disease. *J Neurol Neurosurg Psychiatry* **60**, 78–81.

2 Jones L & Hughes A (2011) Pathogenic mechanisms in Huntington's disease. *Int Rev Neurobiol* **98**, 373–418.

3 Yu S, Mulley J, Loesch D, Turner G, Donnelly A, Gedeon A, Hillen D, Kremer E, Lynch M, Pritchard M *et al.* (1993) A novel gene containing a trinucleotide repeat that is expanded and unstable on Huntington's disease chromosomes. *Cell* **72**, 971–983.

4 Moffitt H, McPhail GD, Woodman B, Hobbs C & Bates GP (2009) Formation of polyglutamine inclusions in a wide range of non-CNS tissues in the HdhQ150 knock-in mouse model of Huntington's disease. *PLoS One* **4**, e8025.

5 Ross AC & Tabrizi SJ (2011) Huntington's disease: from molecular pathogenesis to clinical treatment. *Lancet* **10**, 83–98.

6 Bano D, Zanetti F, Mende Y & Nicotera P (2011) Neurodegenerative processes in Huntington's disease. *Cell Death Dis* **2**, e228.

7 Squitieri F, Falleni A, Cannella M, Orobello S, Fulceri F, Lenzi P & Fornai F (2010) Abnormal morphology of peripheral cell tissues from patients with Huntington disease. *J Neural Transm* **117**, 77–83.

8 van der Burg JM, Björkqvist M & Brundin P (2009) Beyond the brain: widespread pathology in Huntington's disease. *Lancet Neurol* **8**, 765–774.

9 Sorensen SA & Fenger K (1992) Causes of death in patients with Huntington's disease and in unaffected first degree relatives. *J Med Genet* **29**, 911–914.

10 Pattison JS, Sanbe A, Maloyan A, Osinska H, Klevitsky R & Robbins J (2008) Cardiomyocyte expression of a polyglutamine pre-amyloid oligomer causes heart failure. *Circulation* **117**, 2743–2751.

11 Melkani GC, Trujillo AS, Ramos R, Bodmer R, Bernstein SI & Ocorr K (2013) Huntington's disease induced cardiac amyloidosis is reversed by modulating protein folding and oxidative stress pathways in the *Drosophila* heart. *PLoS Genet* **9**, e1004024.

12 Child D, Lee J, Pascua C, Chen Y, Mas Monteys A & Davidson B (2018) Cardiac mTORC1 dysregulation impacts stress adaptation and survival in Huntington's disease. *Cell Rep* **23**, 1020–1033.

13 Schroeder AM, Wang HB, Park S, Jordan MC, Gao F, Coppola G, Fishbein MC, Roos KP, Ghiani CA & Colwell CS (2016) Cardiac dysfunction in the BACHD mouse model of Huntington's disease. *PLoS One* **11**, 1–25.

14 Gray M, Shirasaki DI, Cepeda C, Andre VM, Wilburn B, Lu XH, Tao J, Yamazaki I, Li SH, Sun YE *et al.* (2008) Full-length human mutant huntingtin with a stable polyglutamine repeat can elicit progressive and selective neuropathogenesis in BACHD mice. *J Neurosci* **28**, 6182–6195.

15 Zhang P (2017) CaMKII: the molecular villain that aggravates cardiovascular disease (review). *Exp Ther Med* **13**, 815–820.

16 Hund T & Mohler P (2015) Role of CaMKII in cardiac arrhythmias. *Trends Cardiovasc Med* **25**, 392–397.

17 Gilissen EP & Staneva-dobrovski L (2013) Distinct types of lipofuscin pigment in the hippocampus and cerebellum of aged cheirogaleid primates. *Anat Rec* **296**, 1895–1906.

18 Konopelski P & Ufnal M (2016) Electrocardiography in rats: a comparison to human. *Physiol Res* **65**, 717–725.

19 Cubeddu LX (2003) QT prolongation and fatal arrhythmias: a review of clinical implications and effects of drugs. *Am J Ther* **10**, 452–457.

20 Bers DM (2002) Cardiac excitation–contraction coupling. *Nature* **415**, 198–205.

21 Pogwizd SM & Bers DM (2002) Calcium cycling in heart failure: the arrhythmia connection. *J Cardiovasc Electrophysiol* **13**, 88–91.

22 Bers DM & Guo T (2005) Calcium signaling in cardiac ventricular myocytes. *Ann N Y Acad Sci* **1047**, 86–98.

23 Franz MR, Jamal SM & Narayan SM (2012) The role of action potential alternans in the initiation of atrial fibrillation in humans: a review and future directions. *Europace* **14**, 58–64.

24 Zhao Z, Wen H, Fefelova N, Allen C, Baba A, Matsuda T & Xie L-H (2012) Revisiting the ionic mechanisms of early afterdepolarizations in cardiomyocytes: predominant by Ca waves or Ca currents?. *Am J Physiol Heart Circ Physiol* **302**, H1636–H1644.

25 Venetucci LA, Trafford AW, O'Neill SC & Eisner DA (2008) The sarcoplasmic reticulum and arrhythmogenic calcium release. *Cardiovasc Res* **77**, 285–292.

26 Eisner DA, Kashimura T, O'Neill SC, Venetucci LA & Trafford AW (2009) What role does modulation of the ryanodine receptor play in cardiac inotropy and arrhythmogenesis? *J Mol Cell Cardiol* **46**, 474–481.

27 Mattiazzi A & Kranias EG (2014) The role of CaMKII regulation of phospholamban activity in heart disease. *Front Pharmacol* **5**, 1–11.

28 Rokita AG & Anderson ME (2012) New therapeutic targets in cardiology: arrhythmias and CaMKII. *Circulation* **126**, 2125–2139.

29 Mustroph J, Neef S & Maier LS (2016) CaMKII as a target for arrhythmia suppression. *Pharmacol Ther* **176**, 22–31.

30 Hegyi B, Chen-Izu Y, Jian Z, Shimkunas R, Izu LT & Banyasz T (2015) KN-93 inhibits IKr in mammalian cardiomyocytes. *J Mol Cell Cardiol* **89**, 173–176.

31 Brunk UT & Terman A (2002) The mitochondrial-lysosomal axis theory of aging accumulation of damaged mitochondria as a result of imperfect autophagocytosis. *Eur J Biochem* **269**, 1996–2002.

32 Terman A, Dalen H, Eaton JW, Neuzil J & Brunk UT (2004) Aging of cardiac myocytes in culture: oxidative stress, lipofuscin accumulation, and mitochondrial turnover. *Ann N Y Acad Sci* **1019**, 70–77.

33 Johri A & Beal MF (2012) Antioxidants in Huntington's disease. *Biochim Biophys Acta* **1822**, 664–674.

34 Quintanilla RA & Johnson GVW (2009) Role of mitochondrial dysfunction in the pathogenesis of Huntington's disease. *Brain Res Bull* **80**, 242–247.
35 Shioya T (2007) A simple technique for isolating healthy heart cells from mouse models. *J Physiol Sci* **57**, 327–335.
36 Joviano-Santos J, Santos-Miranda A, Joca H, Cruz J & Ferreira A (2016) New insights into the elucidation of angiotensin-(1-7) in vivo antiarrhythmic effects and its related cellular mechanisms. *Exp Physiol* **101**, 1506–1516.
37 Gioda CR, Barreto TDO, Prímola-gomes TN, De Lima DC, Campos PP, Aggunn S, Lauton-santos S, Vasconcelos AC, Coimbra CC, Soares V *et al.* (2013) Cardiac oxidative stress is involved in heart failure induced by thiamine deprivation in rats. *Am J Physiol Heart Circ Physiol* **298**, 2039–2045.